A&A 485, 71–80 (2008)
DOI: 10.1051/0004-6361:20079298

Astronomy & Astrophysics

Structures in surface-brightness profiles of LMC and SMC star clusters: evidence of mergers?⋆

L. Carvalho[1], T. A. Saurin[1], E. Bica[1], C. Bonatto[1], and A. A. Schmidt[2]

[1] Universidade Federal do Rio Grande do Sul, Departamento de Astronomia, CP 15051, RS, Porto Alegre 91501-970, Brazil
e-mail: [luziane;bica;charles]@if.ufrgs.br; tiago.saurin@ufrgs.br
[2] Universidade Federal de Santa Maria, LANA, RS, Santa Maria 97119-900, Brazil
e-mail: alex@lana.ccne.ufsm.br

Received 20 December 2007 / Accepted 2 April 2008

ABSTRACT

Context. The LMC and SMC are rich in binary star clusters, and some mergers are expected. It is thus important to characterise single clusters, binary clusters and candidates for mergers.
Aims. We selected a sample of star clusters in each Cloud with this aim. Surface photometry of 25 SMC and 22 LMC star clusters was carried with the ESO Danish 1.54 m telescope. 23 clusters were observed for the first time for these purposes.
Methods. We fitted Elson, Fall and Freeman (EFF) profiles to the data, deriving structural parameters, luminosities and masses. We also use isophotal maps to constrain candidates for cluster interactions.
Results. The structural parameters, luminosities and masses presented good agreement with those in the literature. Three binary clusters in the sample have a double profile. Four clusters (NGC 376, K 50, K 54 and NGC 1810) do not have companions and present important deviations from EFF profiles.
Conclusions. The present sample contains blue and red Magellanic clusters. Profiles with excess with respect to EFF were detected in some blue clusters. We find evidence that important deviations from the body of EFF profiles might be used as a tool to detect cluster mergers.

Key words. galaxies: Magellanic Clouds – galaxies: star clusters

1. Introduction

Surface-brightness and number-density profiles can be used to investigate properties of star clusters in different tidal environments. The standard description of Globular Clusters (GCs) assumes an isothermal central region and a tidally truncated outer region (e.g. Binney & Merrifield 1998). However, both structures evolve with time. Evolved GCs, in particular, can be considered as dynamically relaxed systems (e.g. Noyola & Gebhardt 2006). From their formation, star clusters are subject to internal and external processes that affect the spatial distribution of stars and introduce asymmetries in the luminosity distribution, which in principle can be detected by surface-brightness profiles (SBPs). Among the former are mass loss associated with stellar evolution, large-scale mass segregation and low-mass star evaporation. The latter are tidal stress and dynamical friction (e.g. Khalisi et al. 2007; Lamers et al. 2005; Gnedin & Otriker 1997). These processes tend to decrease cluster mass, which may accelerate the core collapse phase in some cases (e.g. Djorgovski & Meylan 1994). With time, what results is a spatial distribution of light (or mass) that reflects the combined effect of these processes associated with physical conditions at the early collapse (Bonatto & Bica 2008, and references therein).

In this context, the present-day internal structure of individual star clusters, as well as the collective large-scale galactocentric distribution can be used to probe conditions related to galaxy formation, and to investigate cluster dynamical evolution (e.g. Mackey & van den Bergh 2005; Bica et al. 2006a).

SBPs of star clusters, GCs in particular, have been shown to follow analytical profiles. The most commonly used are the single-mass, modified isothermal sphere of King (1966) that is the basis of the Galactic GC parameters given by Trager et al. (1995), Harris (1996, and the 2003 update[1]); the modified isothermal sphere of Wilson (1975) that assumes a pre-defined stellar distribution function which results in more extended envelopes than in King (1966), and the power-law with a core of EFF (Elson et al. 1987) that has been fit to massive young clusters especially in the Magellanic Clouds (e.g. Mackey & Gilmore 2003a,b). Each function is characterised by different parameters that are somehow related to the cluster structure. McLaughlin & van der Marel (2005) provided cluster fittings involving these three types of profiles.

Perhaps as interesting as the fact that SBPs can be described by analytical profiles such as King (1966) or EFF, from which structural parameters can be derived, is the fact that significant deviations have been detected. They are (i) post-core-collapse (PCC) excesses to power laws in surface density vs. log radius for Galactic GCs (e.g. Trager et al. 1995) and (ii) in Galactic open clusters (e.g. Bonatto & Bica 2005; Bica et al. 2006b), and (iii) extensions beyond the tidal radius in young populous LMC clusters (e.g. Elson et al. 1987) or R 136 in 30 Dor (e.g. Mackey & Gilmore 2003a), which appear to be related to formation conditions. Noyola & Gebhardt (2006, 2007) detected SBP deviations in central regions of many clusters, including Clouds ones.

Not many SMC clusters have published SBPs. Mackey & Gilmore (2003b) studied 10 populous SMC clusters. Using HST,

⋆ Full Fig. 3 is only available in electronic form at http://www.aanda.org

[1] http://physun.physics.mcmaster.ca/Globular.html

53 clusters in the LMC were studied by Mackey & Gilmore (2003a). Number-density studies (Chrysovergis et al. 1989, and references therein) included SMC and LMC clusters, but inner profiles were limited by the low stellar resolution in photographic material.

Evidence of cluster binarity and mergers has been reported for both Clouds, which appear to be suitable environments for that. Indeed, the SMC and LMC are very rich in cluster pairs and multiplets (Bica & Schmitt 1995; Bica et al. 1999; Dieball et al. 2002). Studies of radial variations of parameters related to isophotes and comparisons with N-body simulations were carried out by de Oliveira et al. (2000a,b), where several possible mergers were discussed. The blue LMC cluster NGC 2214 has been reported as a merger, where the secondary component is still conspicuous in images (Bhatia & MacGillivray 1988). NGC 1846 was shown to be a merger, with two main sequence turn-offs (Mackey & Broby Nielsen 2007).

In the present study we explore a sample of 47 SMC and LMC clusters of different ages, some of them studied in terms of SBP for the first time. The sample selection was mostly based on van den Bergh (1981), to span a wide age range. We argue that distortions found in the SBP of some clusters may arise from the spatial evolution of mergers, and that the star clusters NGC 376, K 50, K 54, and NGC 1810 show evidence of mergers.

This work is structured as follows. In Sect. 2 we present the observations. In Sect. 3 we fit profiles to the data and derive structural parameters and masses. The structures in the profiles are discussed in Sect. 4, and concluding remarks are given in Sect. 5.

2. Observations and analysis

The data were obtained in two observing runs, the first between 1990 November 16 and 20, and the second between 1991 October 25 and November 9 using the ESO Danish 1.54 m telescope, in La Silla, Chile. The detectors were RCA CCDs (SID 501 in the first run and 503 in the second run). They have 320 × 512 and 1024 × 640 pixels, with the spatial scales 0.475″/pixel and 0.237″/pixel (Table 1), respectively. V and B Bessel filters were used. CCD gains were 12.3 and 5.9 electrons/ADU, and readout noises were 31.6 and 15 electrons. The mean seeing for the frames was 1.5″. In Table 1 we summarise the observational data including the exposure time and seeing for each image together with the most common identifiers (Bica & Schmitt 1995; Bica et al. 1999) for the star clusters of this sample.

For all objects the V band observations were used, except NGC 2159, for which the B image had a significantly higher signal-noise ratio.

Figure 1 shows examples of clusters of the present sample. The images are magnifications of the total images with dimension 4.0′ × 2.5′. The first three (NGC 241+242, IC 1612, NGC 2011) are double clusters (Sect. 1). The next three (NGC 376, K 50, NGC 1810) are candidates for mergers (Sect. 4). NGC 346 is a young star cluster embedded in an HII region. NGC 416 is a populous intermediate age SMC cluster, and NGC 1856 is a populous blue LMC cluster.

2.1. Data reduction

All frames were reduced using standard IRAF routines for bias and dark current subtraction and flat-field division. Bad and hot pixels (cosmic rays) were replaced by linear interpolation along lines or columns using the nearest good pixels.

Table 1. Cluster sample and observational details.

Cluster name	Time (s)	Seeing (arcsec)	CCD scale (arcsec/pixel)	Date
(1)	(2)	(3)	(4)	(5)
	SMC			
NGC 121 (K 2, L 10)	360	1.6	0.475	1990
NGC 176 (K 12, L 16)	360	1.6	0.475	1991
K 17 (L 26)	360	1.2	0.475	1991
NGC 241+242 (K 22, L 29)	60	1.7	0.475	1991
NGC 290 (L 42)	60	1.4	0.475	1991
L 48	360	1.8	0.237	1991
K 34 (L 53)	240	1.4	0.475	1991
NGC 330 (K 35, L 54)	100	1.5	0.475	1990
L 56	120	1.6	0.475	1990
NGC 339 (K 36, L 59)	180	1.9	0.475	1990
NGC 346 (L 60)	60	1.8	0.475	1990
IC 1611 (K 40, L 61)	360	1.4	0.475	1991
IC 1612 (K 41, L 62)	360	1.4	0.475	1991
L 66	30	1.3	0.475	1991
NGC 361 (K 46, L 67)	120	1.9	0.475	1991
K 47 (L 70)	120	1.3	0.475	1991
NGC 376 (K 49, L 72)	240	1.5	0.237	1991
K 50 (L 74)	120	1.2	0.475	1991
IC 1624 (K 52, L 76)	180	1.6	0.475	1991
K 54 (L 79)	30	1.9	0.475	1991
NGC 411 (K 60, L 82)	180	2.1	0.475	1991
NGC 416 (K 59, L 83)	150	1.2	0.475	1991
NGC 419 (K 58, L 85)	300	1.4	0.237	1991
NGC 458 (K 69, L 96)	240	1.6	0.475	1990
L 114	180	1.4	0.475	1990
	LMC			
NGC 1783 (SL 148)	300	1.8	0.475	1991
NGC 1810 (SL 194)	120	1.2	0.475	1991
NGC 1818 (SL 201)	60	1.7	0.237	1991
NGC 1831 (SL 227, LW 133)	300	1.6	0.237	1991
NGC 1847 (SL 240)	120	2.2	0.475	1991
NGC 1856 (SL 271)	120	1.7	0.475	1991
NGC 1866 (SL 319, LW 163)	30	1.8	0.475	1990
NGC 1868 (SL 330, LW 169)	120	1.8	0.475	1990
NGC 1870 (SL 317)	120	1.8	0.475	1991
NGC 1978 (SL 501)	160	1.5	0.475	1990
NGC 2004 (SL 523)	60	1.3	0.475	1991
NGC 2011 (SL 559)	160	1.3	0.475	1990
NGC 2100 (SL 662)	20	1.5	0.475	1991
NGC 2121 (SL 725, LW 303)	240	1.3	0.475	1991
NGC 2157 (SL 794)	120	2.1	0.475	1990
NGC 2159 (SL 799)	20	1.3	0.475	1991
NGC 2164 (SL 808)	180	2.2	0.475	1991
NGC 2210 (SL 858, LW 423)	180	1.4	0.475	1991
NGC 2213 (SL 857, LW 419)	120	2.2	0.475	1990
NGC 2214 (SL 860, LW 426)	50	1.8	0.475	1990
H 11 (SL 868, LW 437)	420	1.3	0.475	1991
HS 314	60	1.7	0.475	1990

Notes. Column 1: cluster identifications in main catalogues, Col. 2: CCD exposure time in seconds, Col. 3: seeing in arcseconds, Col. 4: CCD scale in arcseconds per pixel, Col. 5: year of the observing run.

Photometric calibration was performed with a least-squares fit routine that uses errors as weights, with standard stars of Graham (1982) and Landolt (1992), resulting in a mean error smaller than 0.01 mag at a 66% confidence level. The transformations used in the photometric calibration were

$$V = (0.998 \pm 0.006)v + (21.906 \pm 0.074),$$

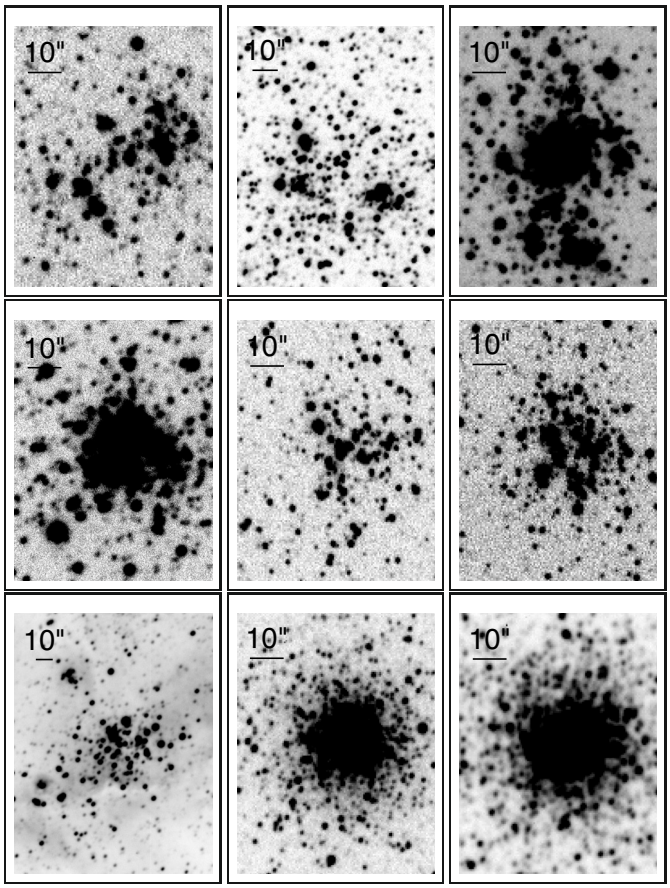

Fig. 1. Central extractions of CCD V band images of examples of the sample clusters. *Top panels* (*left to right*): double clusters NGC 241+242, IC 1612 and NGC 2011. *Middle panels*: merger candidates NGC 376, K 50 and NGC 1810. *Bottom panels*: the young cluster NGC 346 embedded in an HII region, and the populous clusters NGC 416 and NGC 1856. East to *the left and North to the top*.

for the first run, and

$$B = (1.008 \pm 0.013)b + (22.128 \pm 0.118),$$
$$V = (0.985 \pm 0.003)v + (22.304 \pm 0.034),$$

for the second run, where b and v are the instrumental magnitudes. The mean errors are 0.008, 0.014, and 0.006 mag, respectively.

2.1.1. Cluster centre determination

Accurate cluster centres are fundamental, because errors will introduce additional uncertainties in the SBPs. In Fig. 2 we present brightness profiles for an artificial image where we displaced the centre of the surface photometry by 5″, 10″, 15″ and 20″ of the correct centre, successively. It is possible to see that apparently acceptable SBPs can be obtained, although the cluster centre was not determined correctly. However, the resulting structural parameters, especially μ_0, present offsets.

The coordinates of the symmetry centre for each cluster were obtained, with a mean error smaller than 0.5″, using an implementation of the mirror-autocorrelation algorithm (Djorgovski 1988). We obtained for each cluster a set of autocorrelation amplitudes that were fitted with an elliptical paraboloid. The optimal centre is the vertex of this paraboloid.

For some objects we determined the centre by a heuristic method because of their non-symmetrical stellar distribution

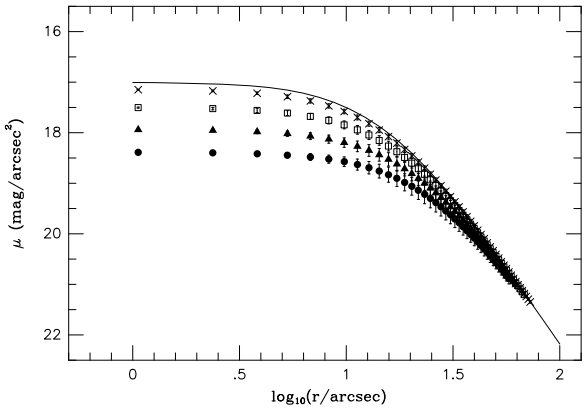

Fig. 2. Example of the effect of the centering error of an object. The solid line represents the brightness distribution of an artificially constructed image. The points represented by crosses were obtained for the centre of the surface photometry displaced by 5″ relative to the centre of the artificial image; squares by 10″; triangles by 15″ and circles by 20″.

as a whole, or the presence of bright stars. This was the case of NGC 241+242, NGC 339, K 47, K 50, NGC 1810, and NGC 2004.

The derived cluster centre positions in equatorial coordinates (J2000) are given in Table 2.

2.2. Surface photometry

Surface photometry was performed with concentric annular apertures centred on the cluster coordinates (Table 2) and subdivided in at least 4, and at most, 32 sectors. An effective radius for each annulus was determined iteractively by following the radial distribution of brightness for each annulus. The counts in each annulus were determined and adopted as surface-brightness, together with its standard deviation. The surface-brightness for each annulus is the mean or median of the values measured for all sectors together with the standard deviation. In Col. 6 of Table 3 we give the adopted statistics. The approach was based on the median. However, for convergence arguments, in some cases we adopted the mean. In general, the median was more suitable for red clusters. A limiting radius of the photometry for each cluster was estimated, so that the rings did not exceed the physical limits of the image.

For each profile, the points are the result of four sets of annuli with radial steps of 1.5″, 2.0″, 3.0″ and 4.0″. Four annulus sets are plotted on the same axes with the best-fitting EFF profile. This is particularly useful to build SBPs with an adequate spatial resolution in the inner regions of the cluster. Conversely, large steps are more suitable for the outer regions. We find that the simultaneous use of four steps yields comparable average profiles.

For each cluster we tested if the mean or the median of the flux in the sectors provided profiles with minimal errors in the surface-brightness and resulting fits. In the luminosity and mass estimates this choice was also important.

The sky level was evaluated considering four peripheral regions in each image that were not affected by the background and field stars. These regions have been merged into a single one, of larger dimension, to compute a self- consistent histogram of sky counts. They were truncated at 3σ of the average until the histogram did not vary any longer. Finally, we chose the mode

Table 2. Cluster centre positions (J2000) determined in this study.

Cluster	α	σ_α	δ	σ_δ
(1)	(2)	(3)	(4)	(5)
	SMC			
NGC 121	$00^h26^m47\overset{s}{.}89$	$0\overset{s}{.}01$	$-71°32'04\overset{''}{.}8$	$0\overset{''}{.}4$
NGC 176	$00^h35^m58\overset{s}{.}18$	$0\overset{s}{.}03$	$-73°09'57\overset{''}{.}7$	$0\overset{''}{.}5$
K 17	$00^h41^m00\overset{s}{.}82$	$0\overset{s}{.}02$	$-72°34'20\overset{''}{.}8$	$0\overset{''}{.}3$
NGC 241	$00^h43^m31\overset{s}{.}61$	$0\overset{s}{.}03$	$-73°26'26\overset{''}{.}8$	$0\overset{''}{.}5$
NGC 290	$00^h51^m14\overset{s}{.}91$	$0\overset{s}{.}02$	$-73°09'40\overset{''}{.}5$	$0\overset{''}{.}4$
L 48	$00^h53^m27\overset{s}{.}60$	$0\overset{s}{.}02$	$-71°23'55\overset{''}{.}1$	$0\overset{''}{.}3$
K 34	$00^h55^m33\overset{s}{.}15$	$0\overset{s}{.}01$	$-72°49'57\overset{''}{.}4$	$0\overset{''}{.}1$
NGC 330	$00^h56^m18\overset{s}{.}30$	$0\overset{s}{.}01$	$-72°27'47\overset{''}{.}9$	$0\overset{''}{.}3$
L 56	$00^h57^m29\overset{s}{.}82$	$0\overset{s}{.}03$	$-72°15'53\overset{''}{.}1$	$0\overset{''}{.}6$
NGC 339	$00^h57^m46\overset{s}{.}04$	$0\overset{s}{.}03$	$-74°28'13\overset{''}{.}2$	$0\overset{''}{.}5$
NGC 346	$00^h59^m05\overset{s}{.}18$	$0\overset{s}{.}04$	$-72°10'38\overset{''}{.}0$	$0\overset{''}{.}4$
IC 1611	$00^h59^m48\overset{s}{.}08$	$0\overset{s}{.}02$	$-72°20'03\overset{''}{.}4$	$0\overset{''}{.}4$
IC 1612	$00^h59^m55\overset{s}{.}31$	$0\overset{s}{.}01$	$-72°22'18\overset{''}{.}6$	$0\overset{''}{.}1$
L 66	$01^h01^m44\overset{s}{.}44$	$0\overset{s}{.}05$	$-72°33'51\overset{''}{.}9$	$0\overset{''}{.}5$
NGC 361	$01^h02^m10\overset{s}{.}48$	$0\overset{s}{.}03$	$-71°36'23\overset{''}{.}3$	$0\overset{''}{.}5$
K 47	$01^h03^m11\overset{s}{.}34$	$0\overset{s}{.}03$	$-72°16'18\overset{''}{.}7$	$0\overset{''}{.}5$
NGC 376	$01^h03^m53\overset{s}{.}63$	$0\overset{s}{.}01$	$-72°49'32\overset{''}{.}9$	$0\overset{''}{.}2$
K 50	$01^h04^m37\overset{s}{.}03$	$0\overset{s}{.}03$	$-72°09'39\overset{''}{.}7$	$1\overset{''}{.}5$
IC 1624	$01^h05^m20\overset{s}{.}92$	$0\overset{s}{.}03$	$-72°02'37\overset{''}{.}3$	$0\overset{''}{.}3$
K 54	$01^h06^m47\overset{s}{.}99$	$0\overset{s}{.}04$	$-72°16'23\overset{''}{.}9$	$0\overset{''}{.}8$
NGC 411	$01^h07^m54\overset{s}{.}34$	$0\overset{s}{.}03$	$-71°46'05\overset{''}{.}6$	$0\overset{''}{.}5$
NGC 416	$01^h07^m59\overset{s}{.}18$	$0\overset{s}{.}02$	$-72°21'19\overset{''}{.}8$	$0\overset{''}{.}2$
NGC 419	$01^h08^m17\overset{s}{.}39$	$0\overset{s}{.}01$	$-72°53'00\overset{''}{.}7$	$0\overset{''}{.}1$
NGC 458	$01^h14^m52\overset{s}{.}29$	$0\overset{s}{.}01$	$-71°33'00\overset{''}{.}2$	$0\overset{''}{.}3$
L 114	$01^h50^m19\overset{s}{.}63$	$0\overset{s}{.}02$	$-74°21'23\overset{''}{.}9$	$0\overset{''}{.}1$
	LMC			
NGC 1783	$04^h59^m08\overset{s}{.}78$	$0\overset{s}{.}03$	$-65°59'17\overset{''}{.}1$	$0\overset{''}{.}3$
NGC 1810	$05^h03^m23\overset{s}{.}31$	$0\overset{s}{.}03$	$-66°22'57\overset{''}{.}3$	$0\overset{''}{.}5$
NGC 1818	$05^h04^m13\overset{s}{.}92$	$0\overset{s}{.}01$	$-66°26'03\overset{''}{.}4$	$0\overset{''}{.}2$
NGC 1831	$05^h06^m16\overset{s}{.}17$	$0\overset{s}{.}01$	$-64°55'10\overset{''}{.}1$	$0\overset{''}{.}2$
NGC 1847	$05^h07^m08\overset{s}{.}16$	$0\overset{s}{.}01$	$-68°58'22\overset{''}{.}6$	$0\overset{''}{.}1$
NGC 1856	$05^h09^m30\overset{s}{.}32$	$0\overset{s}{.}01$	$-69°07'44\overset{''}{.}2$	$0\overset{''}{.}2$
NGC 1866	$05^h13^m38\overset{s}{.}82$	$0\overset{s}{.}03$	$-65°27'55\overset{''}{.}7$	$0\overset{''}{.}2$
NGC 1868	$05^h14^m36\overset{s}{.}09$	$0\overset{s}{.}03$	$-63°57'14\overset{''}{.}8$	$0\overset{''}{.}1$
NGC 1870	$05^h13^m10\overset{s}{.}71$	$0\overset{s}{.}01$	$-69°07'04\overset{''}{.}0$	$0\overset{''}{.}1$
NGC 1978	$05^h28^m44\overset{s}{.}99$	$0\overset{s}{.}02$	$-66°14'10\overset{''}{.}5$	$0\overset{''}{.}4$
NGC 2004	$05^h30^m40\overset{s}{.}34$	$0\overset{s}{.}03$	$-67°17'12\overset{''}{.}8$	$0\overset{''}{.}5$
NGC 2011	$05^h32^m19\overset{s}{.}50$	$0\overset{s}{.}01$	$-67°31'19\overset{''}{.}8$	$0\overset{''}{.}2$
NGC 2100	$05^h42^m07\overset{s}{.}82$	$0\overset{s}{.}02$	$-69°12'40\overset{''}{.}9$	$0\overset{''}{.}3$
NGC 2121	$05^h48^m12\overset{s}{.}71$	$0\overset{s}{.}03$	$-71°28'51\overset{''}{.}7$	$0\overset{''}{.}7$
NGC 2157	$05^h57^m35\overset{s}{.}32$	$0\overset{s}{.}01$	$-69°11'47\overset{''}{.}0$	$0\overset{''}{.}1$
NGC 2159	$05^h58^m03\overset{s}{.}03$	$0\overset{s}{.}03$	$-68°37'30\overset{''}{.}1$	$0\overset{''}{.}5$
NGC 2164	$05^h58^m55\overset{s}{.}88$	$0\overset{s}{.}01$	$-68°30'58\overset{''}{.}3$	$0\overset{''}{.}4$
NGC 2210	$06^h11^m31\overset{s}{.}09$	$0\overset{s}{.}01$	$-69°07'20\overset{''}{.}5$	$0\overset{''}{.}2$
NGC 2213	$06^h10^m42\overset{s}{.}33$	$0\overset{s}{.}01$	$-71°31'45\overset{''}{.}7$	$0\overset{''}{.}1$
NGC 2214	$06^h12^m57\overset{s}{.}24$	$0\overset{s}{.}03$	$-68°15'38\overset{''}{.}1$	$0\overset{''}{.}5$
H 11	$06^h14^m22\overset{s}{.}72$	$0\overset{s}{.}01$	$-69°50'50\overset{''}{.}5$	$0\overset{''}{.}2$
HS 314	$05^h28^m26\overset{s}{.}68$	$0\overset{s}{.}04$	$-68°58'56\overset{''}{.}3$	$0\overset{''}{.}5$

Notes. Column 2: right ascension, Col. 3: standard deviation, Col. 4: declination, Col. 5: standard deviation.

of this distribution as the value of the brightness of the sky and subtracted it from the surface-brightness of the clusters.

We employed the Elson et al. (1987) model to analyse the present cluster sample. Their profiles are well represented by the following model, expressed in magnitudes instead of flux,

$$\mu(r) = \mu_0 + 1.25\gamma \log\left(1 + \frac{r^2}{a^2}\right), \quad (1)$$

where μ_0 is the central surface-brightness in magnitude scale, γ is a dimensionless power-law and a is a parameter that is related to the core radius (r_c) in arcsecs by

$$r_c = a\sqrt{2^{2/\gamma} - 1}. \quad (2)$$

Fits of Eq. (1) were performed with a nonlinear least-squares routine that uses SBP errors as weights. For most of the sample this procedure converged, and the resulting fit parameters are given in Table 3. Exceptions are K 50, K 54 and NGC 1810, for which there was no convergence.

Fits with the 3-parameter King (1966) law provide comparable results to EFF for most young and old clusters in the sample. However, for the old massive clusters such as NGC 121 and H 11 the King profiles provide a tidal radius (20.5 pc and 33.1 pc, respectively). The core radii are 3.1 pc and 3.9 pc, respectively, which are essentially the same as those derived from EFF profiles.

2.2.1. Surface brightness profiles

Surface brightness profiles in magnitude scale for the 47 clusters in the sample are shown in Fig. 3. The fitting radius (r_f) is indicated for each object and these values are listed in Table 4. The clusters NGC 376, K 50, K 54, NGC 1810, could not be fitted by Eq. (1). All profiles were obtained in the V band, except NGC 2159, for which a B image was used.

The variations seen in the profiles do not appear to depend on cluster bright stars, which arise in different age ranges, nor on bright field stars. In order to test this, we cleaned the images of e.g. NGC 330 and NGC 2004 of supergiants, and NGC 2121 of AGB stars. The original and the clean profiles are essentially the same, providing the same parameters, within uncertainties. No bright field star is superimposed on the present clusters.

In addition, since we are dealing with populous clusters, statistical uncertainties are small.

r_f is only a useful concept for determining which points are to be used in a profile fit. It has no underlying physical meaning. There is not a rule for determining r_f because it is affected by different factors, (i) the size of an image compared to a cluster; (ii) contamination of field stars; (iii) spatial inhomogeneity in a cluster. In the present study r_f was selected so that the luminosity that results from the fit presents an acceptable uncertainty. In most cases, several fits were performed before the final r_f was found.

2.3. Luminosity

Integration of Eq. (1) from the centre to the fitting radius r_f yields the luminosity $L(r_f)$:

$$L(r_f) = \frac{2\pi 10^{-0.4\,\mu_0} a^2}{\gamma - 2}\left[1 - \left(1 + \frac{r_f^2}{a^2}\right)^{1-\gamma/2}\right]. \quad (3)$$

For $r_f \to \infty$ and $\gamma > 2$, we have the asymptotic cluster luminosity L_∞:

$$L_\infty = \frac{2\pi 10^{-0.4\,\mu_0} a^2}{\gamma - 2}\,. \quad (4)$$

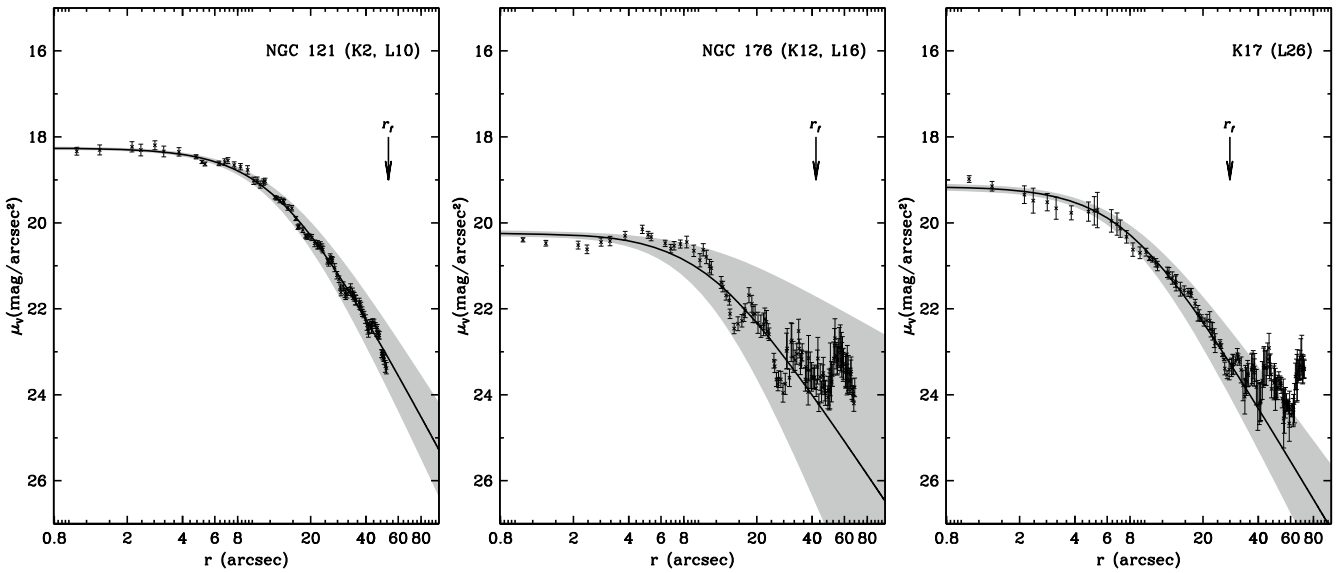

Fig. 3. Surface brightness profiles for the star clusters in the sample. The solid line represents the best fitting EFF model. The shaded line represents the uncertainty of the fit. For each cluster the fitting radius (r_f) is indicated. All profiles are background subtracted.

3. Results

3.1. Structural parameters, luminosity and mass

Table 3 presents the structural parameters obtained by fitting Eq. (1), together with the core radius obtained from the a and γ parameters in Eq. (2).

Luminosity estimates can be obtained by means of Eqs. (3) and (4), both as a function of the fitting radius (r_f), and asymptotic luminosity. Mass estimates have been calculated by multiplying the luminosity by the appropriate mass-to-light ratio. The latter values were obtained (Table 4) from the calibration in Mackey & Gilmore (2003a,b), which are based on the evolutionary synthesis code of Fioc & Rocca-Volmerange (1997) (PEGASE v2.0, 1999).

The calculated values for $L(r_f)$, L_∞, in the V band, $M(r_f)$ and M_∞ are listed in Table 4, together with the fitting radius r_f.

3.2. Comparison with previous studies

Comparison of the values measured in this study with HST results from Mackey & Gilmore (2003a,b) are plotted in Fig. 4. Agreement is in general good. Some deviant points are indicated.

3.3. Comparison of cluster properties

In Fig. 5 we analyse the statistical properties of the present star cluster sample. As a caveat, we note that we are dealing with small fractions of the catalogued star clusters in both Clouds, ≈4.5% in the SMC (Bica & Schmitt 1995) and ≈0.9% in the LMC (Bica et al. 1999). At least for the present sample, the LMC clusters are more massive and luminous than the SMC ones (panels a and b). The age distributions are comparable between the present LMC and SMC clusters (panel c). In terms of radii, both samples present similar distributions (panel d).

In Fig. 6 we investigate relations between parameters. The total luminosity and mass correlate with the core radius (panels d and f), similarly to Galactic open clusters (Bonatto & Bica 2007a). In the present case, the mass reaches about two orders of magnitude higher than in the Galactic ones, while for the core radius the factor is about 4. Despite significant age differences, mass and luminosity correlate (panel e).

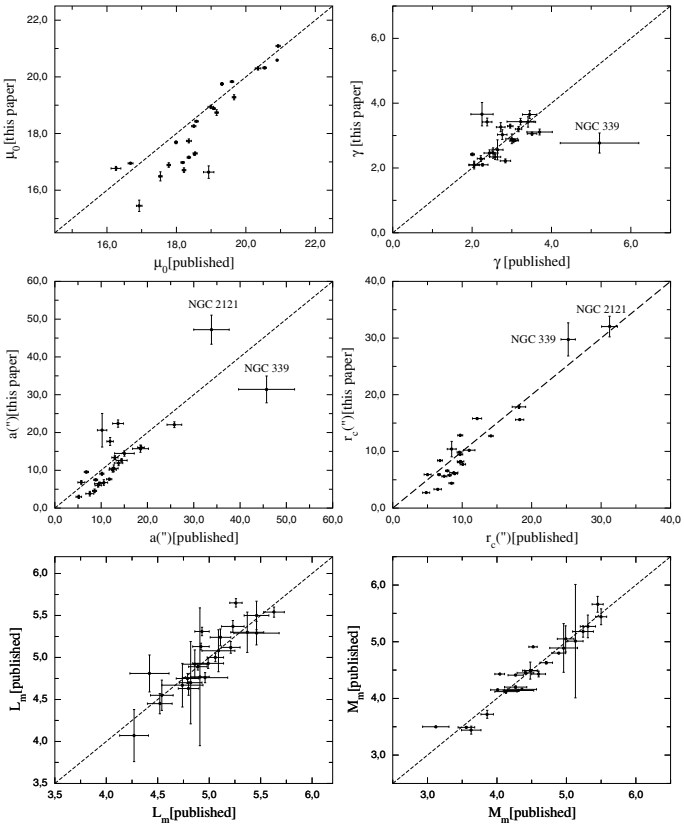

Fig. 4. Measured values of the structural parameters, core radii, luminosity and mass compared with those in common with Mackey & Gilmore (2003a,b). The dashed line is plotted for reference and indicates identity.

Table 3. Structural parameters for the cluster sample derived from the best fitting EFF profiles and core radii.

Cluster	$\mu_{0,V}$ (mag/arcsec^2)	γ	a (arcsec)	r_c (pc)	Adopted statistics
(1)	(2)	(3)	(4)	(5)	(6)
			SMC		
NGC 121	18.26 ± 0.04	3.20 ± 0.08	13.38 ± 0.50	2.81 ± 0.01	median
NGC 176	20.24 ± 0.07	2.56 ± 0.31	10.67 ± 1.59	2.58 ± 0.16	mean
K 17	19.16 ± 0.08	2.87 ± 0.12	7.78 ± 0.54	1.75 ± 0.02	mean
NGC 241+242	17.90 ± 0.17	5.90 ± 3.11	4.76 ± 1.96	0.70 ± 0.09	mean
NGC 290	17.75 ± 0.09	3.09 ± 0.39	6.07 ± 0.97	1.30 ± 0.05	mean
L 48	18.98 ± 0.05	8.55 ± 1.14	15.91 ± 1.69	1.91 ± 0.04	mean
K 34	19.23 ± 0.06	2.48 ± 0.15	9.66 ± 0.82	2.39 ± 0.04	median
NGC 330	16.71 ± 0.09	3.14 ± 0.16	10.41 ± 0.87	2.21 ± 0.04	mean
L 56	16.18 ± 0.10	2.75 ± 0.08	2.94 ± 0.27	0.68 ± 0.01	median
NGC 339	21.18 ± 0.06	3.62 ± 0.25	39.81 ± 2.00	7.76 ± 0.17	mean
NGC 346	17.90 ± 0.11	2.53 ± 0.22	9.68 ± 0.86	2.36 ± 0.05	median
IC 1611	18.98 ± 0.10	2.06 ± 0.19	6.24 ± 1.01	1.75 ± 0.08	median
IC 1612	18.22 ± 0.19	2.13 ± 0.11	2.12 ± 0.32	0.58 ± 0.01	mean
L 66	17.41 ± 0.13	2.76 ± 0.12	3.79 ± 0.37	0.87 ± 0.01	mean
NGC 361	20.32 ± 0.04	2.10 ± 0.08	15.72 ± 0.95	4.34 ± 0.07	median
K 47	19.02 ± 0.05	10.77 ± 3.37	19.35 ± 4.03	2.05 ± 0.20	mean
NGC 376	17.83 ± 0.10	7.96 ± 2.25	15.96 ± 3.33	1.99 ± 0.19	mean
K 50	–	–	–	–	mean
IC 1624	19.64 ± 0.06	2.72 ± 0.16	9.94 ± 0.84	2.31 ± 0.04	median
K 54	–	–	–	–	mean
NGC 411	19.75 ± 0.05	3.26 ± 0.14	17.64 ± 1.05	3.67 ± 0.05	median
NGC 416	18.43 ± 0.02	3.11 ± 0.09	12.63 ± 0.46	2.70 ± 0.01	median
NGC 419	18.25 ± 0.02	2.70 ± 0.06	14.74 ± 0.47	3.45 ± 0.01	median
NGC 458	18.94 ± 0.06	3.43 ± 0.10	14.46 ± 0.73	2.91 ± 0.02	mean
L 114	19.13 ± 0.12	2.40 ± 0.12	3.74 ± 0.40	0.94 ± 0.01	mean
			LMC		
NGC 1783	18.68 ± 0.03	2.72 ± 0.10	21.06 ± 1.00	4.90 ± 0.06	median
NGC 1810	–	–	–	–	mean
NGC 1818	17.16 ± 0.04	3.03 ± 0.15	10.16 ± 0.63	1.88 ± 0.01	median
NGC 1831	18.88 ± 0.02	3.42 ± 0.16	22.07 ± 0.77	3.79 ± 0.02	median
NGC 1847	17.30 ± 0.05	2.09 ± 0.12	4.56 ± 0.49	1.07 ± 0.01	mean
NGC 1856	16.95 ± 0.03	2.42 ± 0.04	9.57 ± 0.27	2.04 ± 0.01	median
NGC 1866	17.27 ± 0.03	2.84 ± 0.06	16.03 ± 0.59	3.09 ± 0.01	mean
NGC 1868	17.69 ± 0.05	2.85 ± 0.03	7.47 ± 0.24	1.44 ± 0.01	mean
NGC 1870	16.38 ± 0.06	3.15 ± 0.07	4.18 ± 0.19	0.76 ± 0.01	median
NGC 1978	18.35 ± 0.03	2.82 ± 0.08	19.67 ± 0.73	3.81 ± 0.02	mean
NGC 2004	15.45 ± 0.20	2.46 ± 0.16	3.82 ± 0.61	0.81 ± 0.02	mean
NGC 2011	16.82 ± 0.20	2.88 ± 0.25	4.53 ± 0.76	0.87 ± 0.02	mean
NGC 2100	16.77 ± 0.07	2.46 ± 0.10	6.80 ± 0.49	1.44 ± 0.01	mean
NGC 2121	20.57 ± 0.04	3.81 ± 0.18	47.80 ± 2.39	7.69 ± 0.16	median
NGC 2157	16.89 ± 0.08	3.65 ± 0.12	11.92 ± 0.69	1.97 ± 0.01	mean
NGC 2159*	19.28 ± 0.09	2.90 ± 0.15	10.52 ± 0.91	2.00 ± 0.03	median
NGC 2164	16.71 ± 0.08	3.29 ± 0.06	9.09 ± 0.40	1.60 ± 0.01	mean
NGC 2210	16.98 ± 0.03	3.06 ± 0.05	7.65 ± 0.25	1.41 ± 0.01	mean
NGC 2213	18.74 ± 0.10	2.22 ± 0.06	6.02 ± 0.48	1.36 ± 0.01	mean
NGC 2214	17.74 ± 0.07	2.10 ± 0.04	6.49 ± 0.36	1.52 ± 0.01	mean
H 11	19.83 ± 0.03	3.42 ± 0.12	22.37 ± 0.97	3.84 ± 0.03	median
HS 314	16.71 ± 0.10	4.46 ± 0.44	5.85 ± 0.69	0.86 ± 0.01	mean

Notes. Column 2: central surface brightness, Col. 3: gamma parameter, Col. 4: a parameter, Col. 5: core radius, Col. 6: statistical adopted for the surface brightness. * For NGC 2159 we used $\mu_{0,B}$.

Core radii (Fig. 6 panel c) show a dependence on age. Finally, mass has a significant correlation with age while luminosity does not (panels b and a, respectively). The mass-age correlation is probably related to dynamical cluster survival. Low mass clusters disperse into the field long before reaching an old age (Goodwin & Bastian 2006).

As compared to Mackey & Gilmore (2003b) similar behaviours occur in the relations in common, especially mass vs. age and core radius vs. age.

The binary clusters in Fig. 6 tend to be among the less massive and with smaller radii in the sample. Note that we measured the main component (Fig. 3).

4. Atypical Magellanic clusters

4.1. Extended profile in the very young cluster NGC 346

The giant SMC HII region cluster NGC 346 (Fig. 1) has a systematic density excess for $r > 10''$ (Fig. 3), as has R 136 in

Table 4. Luminosity in the V band and mass estimate calculated using structural parameters.

Cluster	Age (Gyr)	Ref.	r_f (pc)	M/L_V	$\log L_f$ ($L_{\odot,V}$)	$\log L_\infty$ ($L_{\odot,V}$)	$\log M_f$ ($M_\odot$)	$\log M_\infty$ ($M_\odot$)
(1)	(2)	(3)	(4)	(5)	(6)	(7)	(8)	(9)
SMC								
NGC 121	11.90 ± 1.30	2	12.88	2.74	5.08 ± 0.05	5.17 ± 0.05	5.52 ± 0.14	5.61 ± 0.13
NGC 176	0.46 ± 0.01	3	10.20	0.23	4.25 ± 0.34	4.51 ± 0.27	3.61 ± 0.08	3.87 ± 0.06
K 17	0.30 ± 0.10	9	6.80	0.28	4.31 ± 0.10	4.48 ± 0.09	3.76 ± 0.03	3.93 ± 0.03
NGC 241+242	0.07 ± 0.04	10	1.46	0.17	3.83 ± 0.56	3.90 ± 0.50	3.06 ± 0.10	3.13 ± 0.09
NGC 290	0.03 ± 0.01	14	4.86	0.10	4.60 ± 0.24	4.73 ± 0.21	3.60 ± 0.02	3.73 ± 0.02
L 48	0.15 ± 0.04	3	5.83	0.20	4.29 ± 0.13	4.30 ± 0.12	3.59 ± 0.03	3.60 ± 0.02
K 34	0.24 ± 0.12	10	11.42	0.22	4.60 ± 0.19	4.90 ± 0.16	3.94 ± 0.04	4.24 ± 0.03
NGC 330	0.03 ± 0.01	1	9.72	0.09	5.49 ± 0.11	5.59 ± 0.10	4.45 ± 0.01	4.55 ± 0.01
L 56	0.006 ± 0.01	14	8.75	0.14	4.82 ± 0.10	4.89 ± 0.10	3.96 ± 0.01	4.04 ± 0.01
NGC 339	6.30 ± 1.30	2	19.98	1.66	4.65 ± 0.11	4.82 ± 0.08	4.87 ± 0.18	5.04 ± 0.14
NGC 346	∼0.003	17	2.92	0.02	4.73 ± 0.28	5.39 ± 0.20	3.03 ± 0.01	3.69 ± 0.01
IC 1611	0.11 ± 0.05	10	9.23	0.16	4.54 ± 1.95	5.52 ± 1.38	3.74 ± 0.31	4.72 ± 0.22
IC 1612	∼0.10	16	3.89	0.14	3.92 ± 0.53	4.55 ± 0.40	3.06 ± 0.07	3.70 ± 0.06
L 66	0.15 ± 0.10	11	6.32	0.08	4.50 ± 0.12	4.61 ± 0.12	3.40 ± 0.01	3.52 ± 0.01
NGC 361	8.10 ± 1.20	2	19.13	2.03	4.70 ± 0.49	5.57 ± 0.35	5.01 ± 1.00	5.87 ± 0.71
K 47	∼0.007	16	4.86	0.10	4.30 ± 0.29	4.32 ± 0.25	3.30 ± 0.03	3.32 ± 0.02
NGC 376	∼0.016	16	4.62	0.09	4.77 ± 0.29	4.80 ± 0.25	3.72 ± 0.03	3.75 ± 0.02
K 50	∼0.008	16	–	–	–	–	–	–
IC 1624	0.06 ± 0.03	10	9.72	0.12	4.39 ± 0.14	4.58 ± 0.12	3.47 ± 0.02	3.66 ± 0.01
K 54	∼0.10	16	–	–	–	–	–	–
NGC 411	0.20 ± 0.10	3	15.91	0.63	4.70 ± 0.08	4.79 ± 0.07	4.50 ± 0.05	4.59 ± 0.05
NGC 416	6.90 ± 1.10	2	14.58	1.79	5.00 ± 0.06	5.09 ± 0.05	5.26 ± 0.10	5.34 ± 0.09
NGC 419	∼0.40	16	15.18	0.40	5.30 ± 0.06	5.49 ± 0.05	4.90 ± 0.02	5.09 ± 0.02
NGC 458	0.05 ± 0.01	3	17.01	0.25	4.84 ± 0.06	4.89 ± 0.06	4.24 ± 0.02	4.29 ± 0.01
L 114	5.60 ± 0.50	14	12.15	0.20	4.00 ± 0.19	4.19 ± 0.17	3.30 ± 0.04	3.49 ± 0.03
LMC								
NGC 1783	1.30 ± 0.40	4	20.41	0.63	5.39 ± 0.09	5.62 ± 0.07	5.19 ± 0.06	5.42 ± 0.05
NGC 1810	0.05 ± 0.04	3	–	–	–	–	–	–
NGC 1818	0.02 ± 0.01	3	9.72	0.08	5.24 ± 0.10	5.36 ± 0.08	4.15 ± 0.01	4.26 ± 0.01
NGC 1831	0.32 ± 0.12	4	17.25	0.32	5.12 ± 0.07	5.21 ± 0.06	4.63 ± 0.02	4.71 ± 0.02
NGC 1847	0.02 ± 0.01	3	4.86	0.09	4.77 ± 0.82	5.67 ± 0.59	3.72 ± 0.07	4.62 ± 0.05
NGC 1856	0.12 ± 0.04	4	18.10	0.18	5.54 ± 0.06	5.78 ± 0.05	4.80 ± 0.01	5.04 ± 0.01
NGC 1866	0.09 ± 0.01	7	17.01	0.18	5.65 ± 0.05	5.80 ± 0.05	4.91 ± 0.01	5.06 ± 0.01
NGC 1868	0.33 ± 0.03	3	15.79	0.40	4.89 ± 0.04	4.96 ± 0.04	4.49 ± 0.02	4.57 ± 0.02
NGC 1870	0.72 ± 0.30	19	5.83	0.16	4.79 ± 0.06	4.85 ± 0.05	3.99 ± 0.01	4.06 ± 0.01
NGC 1978	2.50 ± 0.50	18	16.52	2.10	5.37 ± 0.07	5.56 ± 0.05	5.69 ± 0.14	5.88 ± 0.11
NGC 2004	0.03 ± 0.01	4	5.83	0.08	5.30 ± 0.24	5.54 ± 0.22	4.20 ± 0.02	4.45 ± 0.02
NGC 2011	<0.01	6	5.83	0.05	4.75 ± 0.21	4.86 ± 0.21	3.45 ± 0.01	3.56 ± 0.01
NGC 2100	0.032 ± 0.019	4	11.66	0.07	5.29 ± 0.14	5.52 ± 0.12	4.14 ± 0.01	4.36 ± 0.01
NGC 2121	0.70 ± 0.20	3	18.10	1.33	4.92 ± 0.10	5.10 ± 0.06	5.05 ± 0.13	5.22 ± 0.08
NGC 2157	0.03 ± 0.02	3	14.58	0.11	5.37 ± 0.07	5.40 ± 0.07	4.41 ± 0.01	4.44 ± 0.01
NGC 2159*	0.06 ± 0.03	3	9.72	–	–	–	–	–
NGC 2164	0.05 ± 0.03	3	17.98	0.13	5.31 ± 0.05	5.34 ± 0.05	4.43 ± 0.01	4.46 ± 0.01
NGC 2210	15.85 ± 1.26	13	17.01	3.37	5.13 ± 0.04	5.17 ± 0.04	5.66 ± 0.14	5.70 ± 0.12
NGC 2213	1.30 ± 0.50	5	15.55	0.87	4.55 ± 0.18	4.94 ± 0.14	4.49 ± 0.15	4.88 ± 0.12
NGC 2214	0.04 ± 0.01	3	17.01	0.11	5.08 ± 0.25	5.75 ± 0.18	4.12 ± 0.03	4.79 ± 0.02
H 11	15.00 ± 3.00	8	17.74	3.25	4.75 ± 0.06	4.84 ± 0.05	5.27 ± 0.20	5.35 ± 0.18
HS 314	<0.01	15	4.13	0.03	4.65 ± 0.14	4.68 ± 0.13	3.13 ± 0.01	3.16 ± 0.01

Notes. Column 2: cluster age, Col. 3: age reference, Col. 4: fitting radius, Col. 5: mass-to-light radius, Col. 6: mass in fitting radius, Col. 7: asymptotic mass, Col. 8: luminosity in the fitting radius, Col. 9: asymptotic luminosity. (1) Da Costa & Hatzidimitriou (1998); (2) Mighell et al. (1998); (3) Hodge (1983); (4) Santos & Piatti (2004); (5) Da Costa et al. (1985); (6) Gouliermis et al. (2006); (7) Becker & Mathews (1983); (8) Mighell et al. (1996); (9) Hodge & Flower (1987); (10) Elson & Fall (1985); (11) Piatti et al. (2005); (12) Piatti et al. (2005); (13) Geisler et al. (1997); (14) Ahumada et al. (2002); (15) Bica et al. (1996); (16) Chiosi et al. (2006); (17) Sabbi & Sirianni (2008); (18) Sagar & Pandey (1989); (19) Alcaino & Liller (1987). * A B image was used.

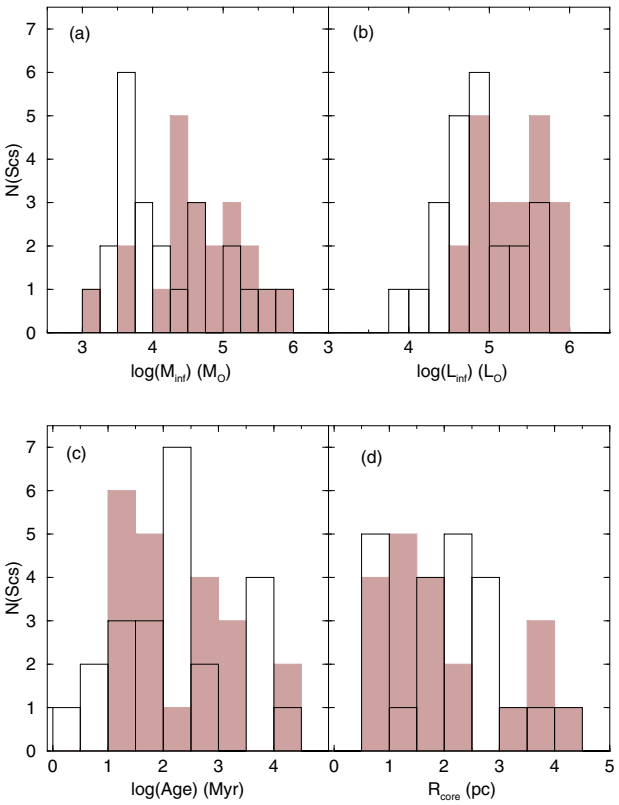

Fig. 5. Comparison between LMC (shaded histograms) and SMC (empty) star clusters. Parameters are from Tables 3 and 4.

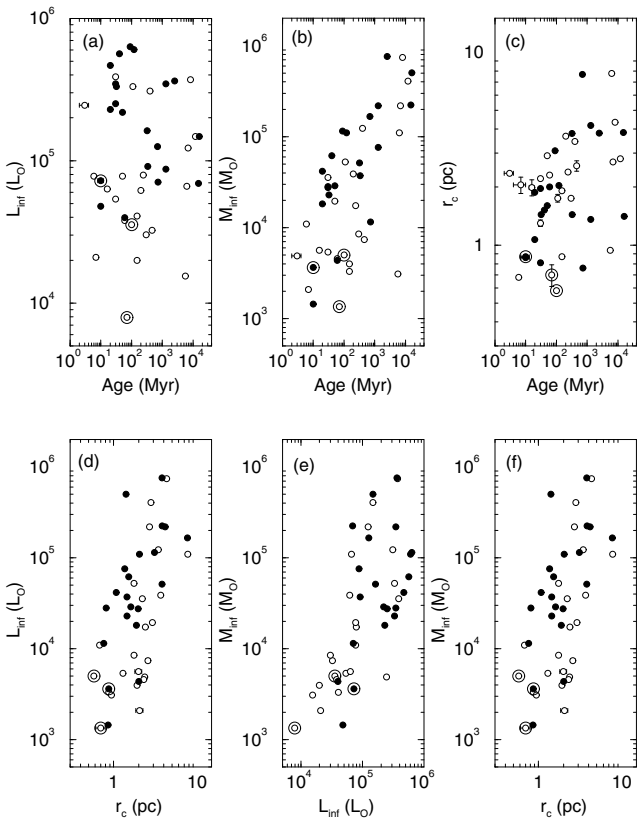

Fig. 6. Relations between cluster parameters. Open circles are SMC and filled circles are LMC clusters. Binary clusters are encircled.

30 Doradus (Mackey & Gilmore 2003a). This may be attributed to star formation in a dynamically infant cluster. The excess in NGC 346 is not a contamination by the neighbouring intermediate age cluster BS 90 (Bica & Schmitt 1995; Rochau et al. 2007). The adopted r_f of NGC 346 is the largest one possible whose fit results in a physically meaningful luminosity.

4.2. Binary clusters and merger candidates

We show in Fig. 7 isophotal maps for the binary clusters and merger candidates in the present sample. We applied Gaussian filters to smooth the images using the *gauss* routine of the IRAF/IMFILTER package.

At least three brightest stars per cluster were removed for NGC 376, K 50, K 54 and NGC 1810. The SBPs remained essentially the same as in the original profiles (Fig. 3). The isophotal maps (Fig. 7) are more sensitive for this removal, but features like double peaks, gaps and triangular or elongated shapes remain. Mackey & Gilmore (2003a) pointed out that bright stars cannot explain bumps observed in SBPs of Magellanic Clouds clusters.

The clusters NGC 376, K 50 and K 54 do not have a detected companion, and NGC 1810 has an unusual profile (Fig. 3). EFF profiles do not describe them. Their isophotal maps may show gaps and/or triangular shapes. In particular NGC 1810 presents an isophotal gap that extends towards the cluster central parts (Fig. 7 panel g).

As it became clear in the analysis of Fig. 3, seven clusters could not be satisfactorily fitted with EFF profiles due to the presence of large-scale structures along the SBPs. NGC 241+242 and IC 1612 + H86−186 are binary clusters in the SMC (de Oliveira et al. 2000a), while NGC 2011 + BRHT14b is a binary cluster in the LMC (Bhatia et al. 1991; Dieball et al. 2002; Gouliermis et al. 2006). The double bump representing the cluster members can be seen in the profiles (Fig. 3). Isophotal maps of NGC 241+242, IC 1612 and NGC 2011 support this in Fig. 7.

In the numerical simulations of cluster encounters by de Oliveira et al. (2000b), similar structures can be seen. We conclude that unusual cluster profiles and isophotal distributions may be related to star cluster mergers.

4.3. Extended profiles

The SMC clusters NGC 176, NGC 290, L 66, K 47, IC 1624, and the LMC clusters NGC 1870, NGC 2159 and HS 314, in particular, have extensions beyond the EFF fitted profiles (Fig. 3). We are dealing with Blue Magellanic Clusters, with ages as a rule younger than 500 Myr and such clusters do not seem to be tidally truncated. Expansion due to mass loss or violent relaxation in the early cluster may contribute. The present work (Sect. 4.2) suggests that cluster interactions and eventual mergers may also contribute to clusters exceeding the Roche limit.

Atypically bright stars in the background area were removed using the IRAF/DAOPHOT package, but the extensions remain. These extensions are not due to contamination by field stars, because they occupy very limited regions of the radius profiles.

Table 5 summarises the main conclusions about structures observed in the profiles of the star clusters of this study, including finer details. Note that objects in common with Mackey & Gilmore (2003a,b) have similar fine structures in the profile (e.g. NGC 176, Fig. 3). It is interesting that 35 of the clusters appear to have at least one significant fine structure (~2 pc of typical size) in the observed light profiles. The seeing (Sect. 2) implies a resolution better than 0.5 pc. The fine structure occurs on a smaller

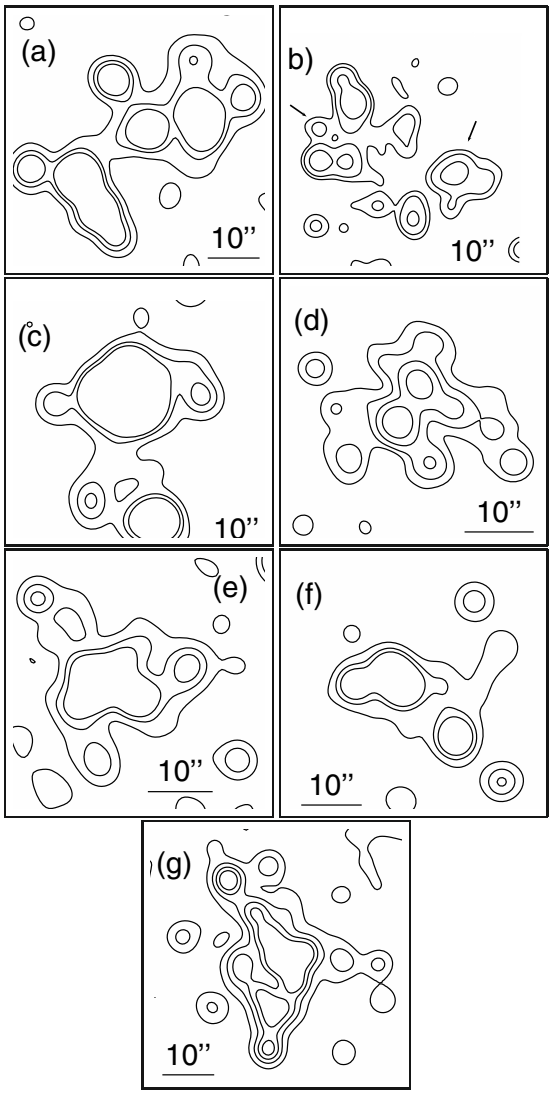

Fig. 7. Intensity isophotal maps of **a)** NGC 241+242, **b)** IC 1612 (components are marked), **c)** NGC 2011, **d)** NGC 376, **e)** K 50, **f)** K 54 and **g)** NGC 1810. Atypically bright stars were removed for NGC 376, K 50, K 54 and NGC 1810.

spatial scale than the larger variations (∼5 pc) observed in the profile of the four clusters with evidence of mergers (Sect. 4.2).

We measured the background and bumps (Table 6) for the clusters listed with “bump” in Table 5. Objects with significant excess (1-σ) are indicated in the last column. In particular L 114, a young cluster in the bridge connecting the Clouds, appears to have a prominent excess or corona.

Table 5. Structures in the profiles.

Cluster	Internal profile	External profile	Diagnostic
(1)	(2)	(3)	(4)
	SMC		
NGC 121	NP	–	–
NGC 176	RD+	bump	–
K 17	RD	bump	–
NGC 241+242	–	–	binary
NGC 290	RD+	bump	–
L 48	RD	bump	–
K 34	NP	bump	–
NGC 330	RD	bump	–
L 56	RD	bump	–
NGC 339	RD	–	–
NGC 346	RD	–	–
IC 1611	NP	–	–
IC 1612	–	bump	binary
L 66	RD	bump	–
NGC 361	NP	–	–
K 47	NP	bump	–
NGC 376	RD++	bump	merger
K 50	RD++	bump	merger
IC 1624	RD	bump	–
K 54	RD++	–	merger
NGC 411	NP	–	–
NGC 416	NP	–	–
NGC 419	NP	–	–
NGC 458	RD+	–	–
L 114	RD+	bump	–
	LMC		
NGC 1783	NP	–	–
NGC 1810	RD++	bump	merger
NGC 1818	RD	–	–
NGC 1831	NP	–	–
NGC 1847	NP	bump	–
NGC 1856	NP	–	–
NGC 1866	RD	–	–
NGC 1868	NP	–	–
NGC 1870	NP	bump	–
NGC 1978	NP	–	–
NGC 2004	RD	–	–
NGC 2011	RD+	bump	binary
NGC 2100	RD	–	–
NGC 2121	NP	–	–
NGC 2157	NP	–	–
NGC 2159	RD+	bump	–
NGC 2164	RD	–	–
NGC 2210	NP	–	–
NGC 2213	RD	–	–
NGC 2214	RD	–	–
H 11	NP	–	–
HS 314	RD+	bump	–

Notes. Column 2: characterisation of internal profiles, Col. 3: characterisation of external profiles, Col. 4: final diagnostic. NP: normal profile, RD: radially disturbed. Plus sign suggests intensity.

5. Concluding remarks

Surface brightness profiles in the V band were derived for 25 SMC and 22 LMC star clusters, including blue and red ones.

Cluster centres were determined using the mirror autocorrelation (Djorgovski 1988) method with a mean error smaller than 0.5″.

The observed profiles were fitted with the EFF model. The structural parameters obtained from the fits were used to determine luminosities and masses of the star clusters. For those in common with the HST study of Mackey & Gilmore (2003a,b) the agreement is good. For 23 objects the analysis is carried out for the first time.

It is important to characterise single clusters, binary and candidates for mergers in the Clouds, which are ideal laboratories for dynamical studies.

In some cases, the profiles present important deviations from EFF profiles. We also use isophotal maps to constrain candidates to cluster interactions. The binary clusters NGC 241+242,

Table 6. The clusters with bumps in the outer extensions. Comparison between the mean values of the bump and the background.

Cluster	Background (mag/arcsec^2)	Bump (mag/arcsec^2)	Excess
(1)	(2)	(3)	(4)
	SMC		
NGC 176	24.6 ± 0.9	23.4 ± 0.3	–
K 17	25.0 ± 0.4	23.7 ± 0.4	–
NGC 241+242	23.1 ± 0.3	22.6 ± 0.3	
NGC 290	23.1 ± 0.7	21.8 ± 0.6	EE
L 48	24.7 ± 0.2	24.3 ± 0.5	–
K 34	22.9 ± 0.6	22.9 ± 0.2	–
NGC 330	23.1 ± 0.4	21.5 ± 0.5	EE
L 56	23.6 ± 0.3	23.3 ± 0.2	EE
IC 1612	23.6 ± 0.3	22.3 ± 0.4	EE
L 66	23.1 ± 0.4	22.5 ± 0.5	–
K 47	23.6 ± 0.6	22.7 ± 0.5	EE
NGC 376	23.8 ± 0.6	22.0 ± 0.6	EE
K 50	23.8 ± 0.3	22.8 ± 0.4	EE
IC 1624	24.2 ± 0.3	23.3 ± 0.5	EE
K 54	23.2 ± 0.4	22.2 ± 0.5	EE
L 114	26.2 ± 0.2	24.6 ± 0.5	EE
	LMC		
NGC 1810	24.2 ± 0.2	23.1 ± 0.6	EE
NGC 1847	23.4 ± 0.3	22.0 ± 0.4	EE
NGC 1870	22.5 ± 0.4	22.6 ± 0.5	–
NGC 2011	24.6 ± 0.6	22.1 ± 0.6	EE
NGC 2159	23.3 ± 0.2	21.9 ± 0.1	EE
HS 314	23.0 ± 0.5	22.1 ± 0.3	EE

Notes. Column 2: background mean, Col. 3: bump mean, Col. 4: presence of external excess. EE: external excess.

IC 1612, and NGC 2011 have a double profile. The clusters NGC 376, K 50, K 54 and NGC 1810 do not have detected companions and present as well significant deviations from EFF profiles with bumps and dips on a ∼5 pc scale.

We conclude that important deviations from the body of EFF profiles might be used as a tool to detect cluster mergers.

Acknowledgements. We thank the anonymous referee for helpful suggestions. We acknowledge partial support from the Brazilian Institution CNPq.

References

Alcaino, G., & Liller, W. 1987, AJ, 94, 372
Ahumada, A. V., Claria, J. J., Bica, E., & Dutra, C. M. 2002, A&A, 393, 855
Becker, S. A., & Mathews, G. J. 1983, ApJ, 270, 155
Bhatia, R. K., & MacGillivray, H. T. 1988, A&A, 203, L5
Bhatia, R. K., Read, M. A., Tritton, S., & Hatzidimitriou, D. 1991, A&AS, 87, 335
Bica, E., & Schmitt, H. R. 1995, ApJS, 101, 41
Bica, E., Claria, J. J., Dottori, H., Santos, J. F. C., Jr., & Piatti, A. E. 1996, ApJS, 102, 57
Bica, E., Schmitt, H. R., Dutra, C. M., & Oliveira, H. L. 1999, AJ, 117, 238
Bica, E., Bonatto, C., Barbuy, B., & Ortolani, S. 2006a, A&A, 450, 105
Bica, E., Bonatto, C., & Blumberg, R. 2006b, A&A, 460, 83
Binney, J., & Merrifield, M. 1998, in Galactic Astronomy (Princeton, NJ: Princeton University Press), Princeton series in Astrophysics
Bonatto, C., & Bica, E. 2005, A&A, 437, 483
Bonatto, C., & Bica, E. 2007a, MNRAS, 377, 1301
Bonatto, C. & Bica, E. 2007b, A&A, 473, 445
Bonatto, C., & Bica, E. 2008, A&A, 477, 829
Chiosi, E., Vallenari, A., Held, E. V., Rizzi, L., & Moretti, A. 2006, A&A, 452, 179
Chrysovergis, M., Kontizas, M., & Kontizas, E. 1989, A&AS, 77, 235
Da Costa, G. S., & Hatzidimitriou, D. 1998, AJ, 115, 1934
Da Costa, G. S., Mould, J. R., & Crawford, M. D. 1985, ApJ, 297, 582
de Oliveira, M. R., Dutra, C. M., Bica, E., & Dottori, H. 2000a, A&A, 146, 57
de Oliveira, M. R., Bica, E., & Dottori, H. 2000b, MNRAS, 311, 589
Dieball, A., Müller, H., & Grebel, E. K. 2002, A&A, 391, 547
Djorgovski, S. 1988, The Harlow-Shapley Symposium on Globular Cluster Systems in Galaxies; Proceedings of the 126th IAU Symp., 126, 333
Djorgovski, S., & Meylan, G. 1994, AJ, 108, 1292
Elson, R. A. W. 1991, ApJS, 76, 185
Elson, R. A. W. 1992, MNRAS, 256, 515
Elson, R. A. W., & Fall, S. M. 1985, ApJ, 299, 211
Elson, R. A. W., Fall, S. M., & Freeman, K. C. 1987, ApJ, 323, 54
Elson, R. A. W., Freeman, K. C., & Lauer, T. R. 1989, ApJ, 347, L69
Fioc, M., & Rocca-Volmerange, B. 1997, A&A, 326, 950
Geisler, D., Bica, E., Dottori, H., et al. 1997, AJ, 114, 1920
Gnedin, O. Y., & Otriker, J. P. 1997, ApJ, 474, 223
Goodwin, S. P., & Bastian, N. 2006, MNRAS, 373, 752
Gouliermis, D. A., Lianou, S., Kontizas, M., Kontizas, E., & Dapergolas, A. 2006, ApJ, 652, 93
Graham, J. A. 1982, PASP, 94, 244
Harris, W. E. 1996, AJ, 112, 1487
Hodge, P. W. 1983, ApJ, 264, 470
Hodge, P. W., & Flower, P. 1987, PASP, 99, 734
Khalisi, E., Amaro-Seoane, P., & Spurzem, R. 2007, MNRAS, 374, 703
King, I. R. 1966, AJ, 71, 64
Lamers, H. J. G. L. M., Gieles, M., Bastian, N., et al. 2005, A&A, 441, 117
Landolt, A. U. 1992, AJ, 340, 104
Mackey, A. D., & Gilmore, G. F. 2003a, MNRAS, 338, 85
Mackey, A. D., & Gilmore, G. F. 2003b, MNRAS, 338, 120
Mackey, A. D., & van den Bergh, S. 2005, MNRAS, 360, 631
Mackey, A. D., & Broby Nielsen, P. 2007, MNRAS, 379, 151
McLaughlin, D. E., & van der Marel, R. P. 2005, ApJS, 161, 304
Mateo, M. 1987, ApJ, 323, L41
Mighell, K. J., Rich, R. M., Shara, M., & Fall, S. M. 1996, AJ, 111, 2314
Mighell, K. J., Sarajedini, A., & French, R. S. 1998, AJ, 116, 2395
Noyola, E., & Gebhardt, K. 2006, AJ, 132, 447
Noyola, E., & Gebhardt, K. 2007, AJ, 134, 912
Piatti, A. E., Santos Jr., J. F. C., Claria, J. J., et al. 2005, A&A, 440, 111
Rochau, D., Gouliermis, D. A., Brandner, W., Dolphin, A. E., & Henning, T. 2007, ApJ, 664, 322
Sabbi, E., Sirianni, M., Nota, A., et al. 2008, AJ, 135, 173
Sagar, R., & Pandey, A. K. 1989, A&AS, 79, 407
Santos, J. F. C., Jr., & Piatti, A. E. 2004, A&A, 428, 79
Trager, S. C., King, I. R., & Djorgovski, S. 1995, AJ, 109, 218
van den Bergh, S. 1981, A&AS, 46, 79
Wilson, C. P. 1975, AJ, 80, 175

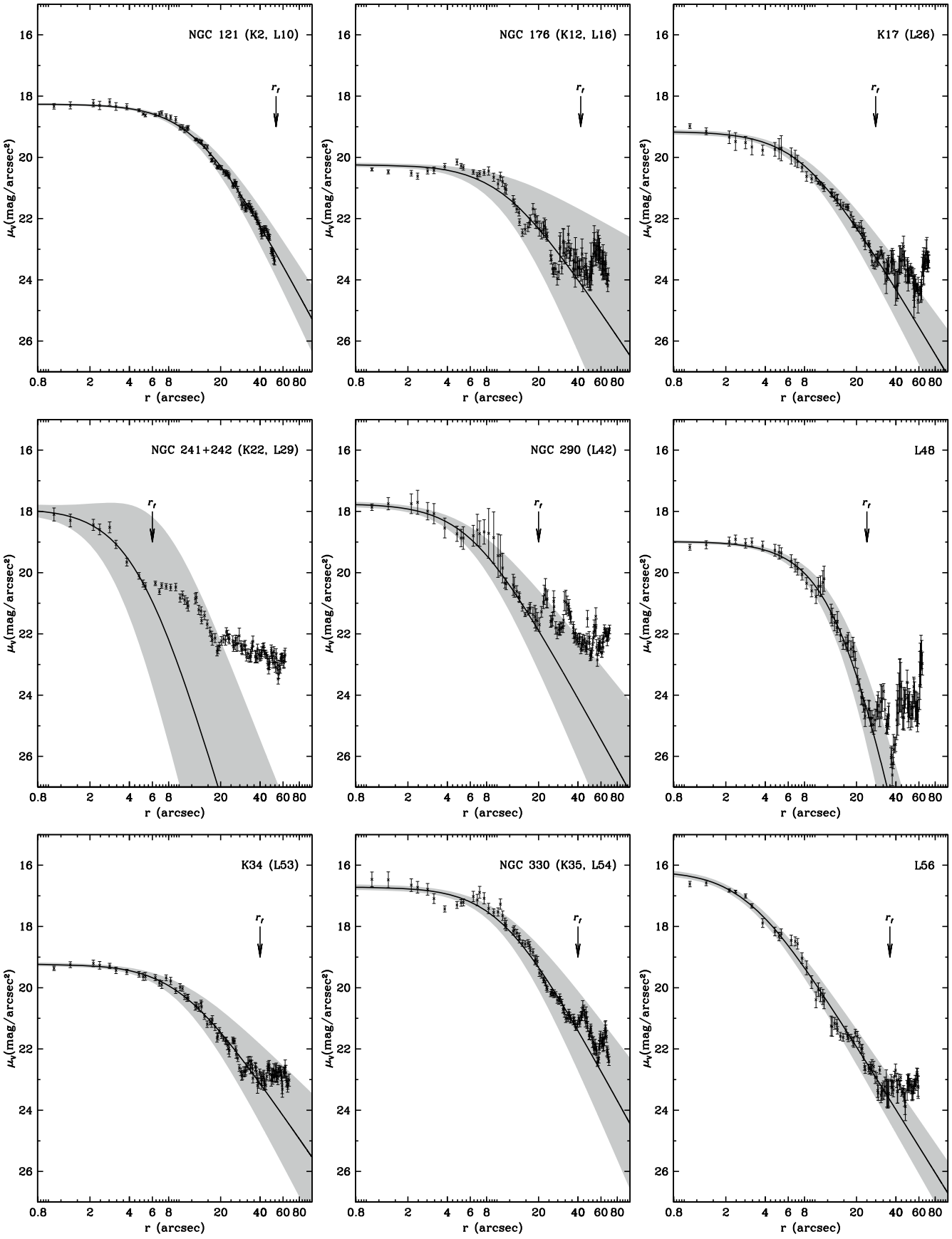

Fig. 3. Surface brightness profiles for the star clusters in the sample. The solid line represents the best fitting EFF model. The shaded line represents the uncertainty of the fit. For each cluster the fitting radius (r_f) is indicated. All profiles are background subtracted.

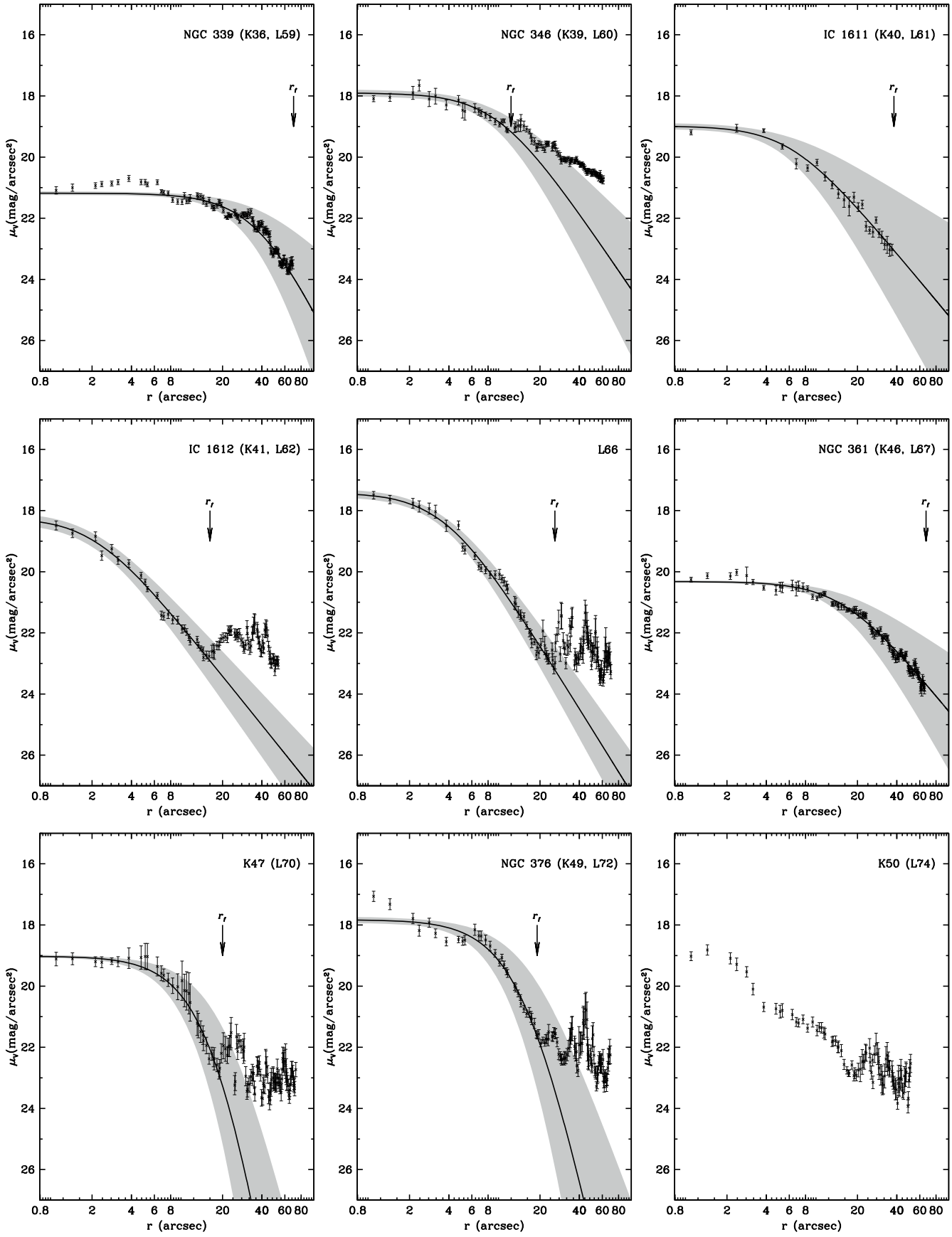

Fig. 3. continued.

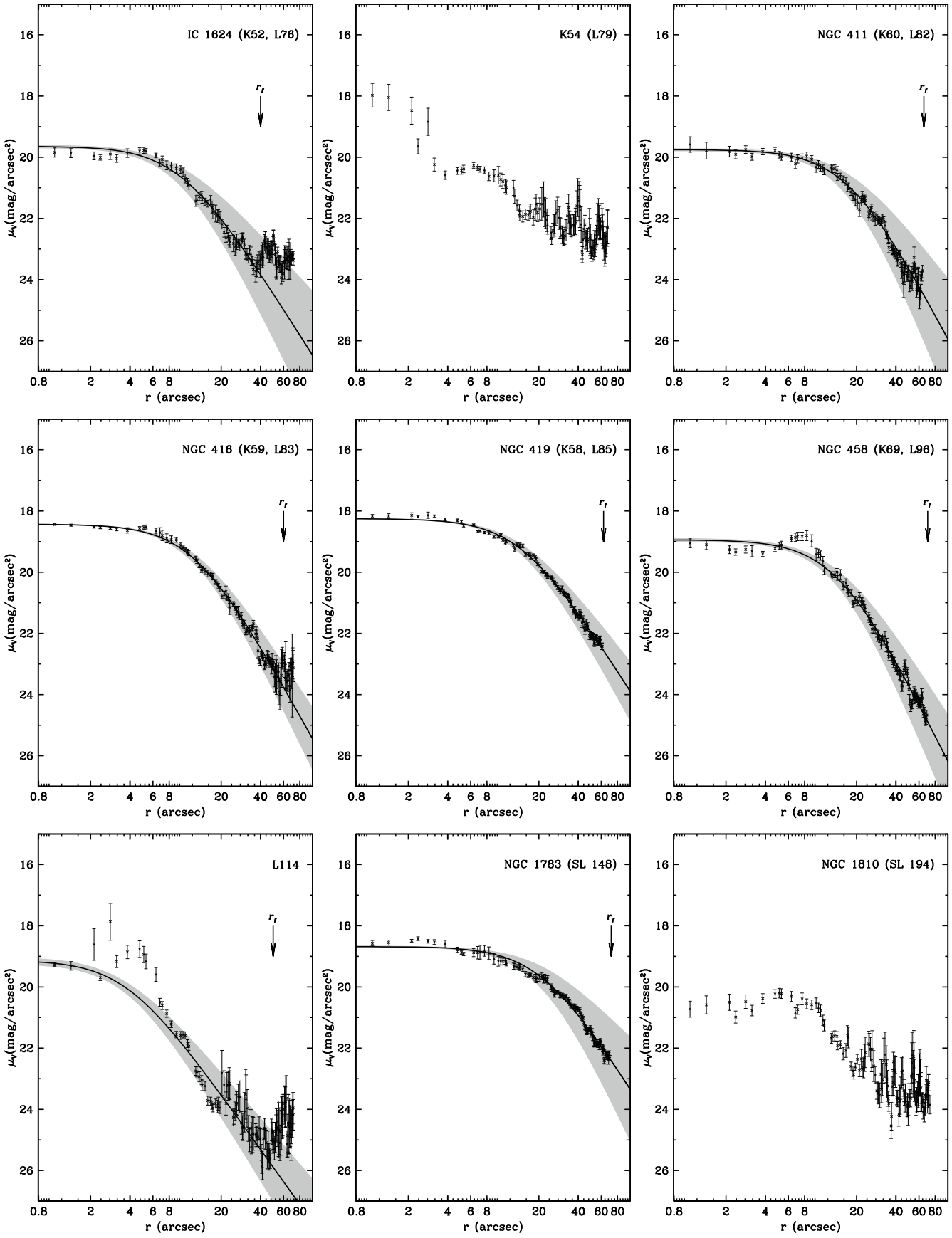

Fig. 3. continued.

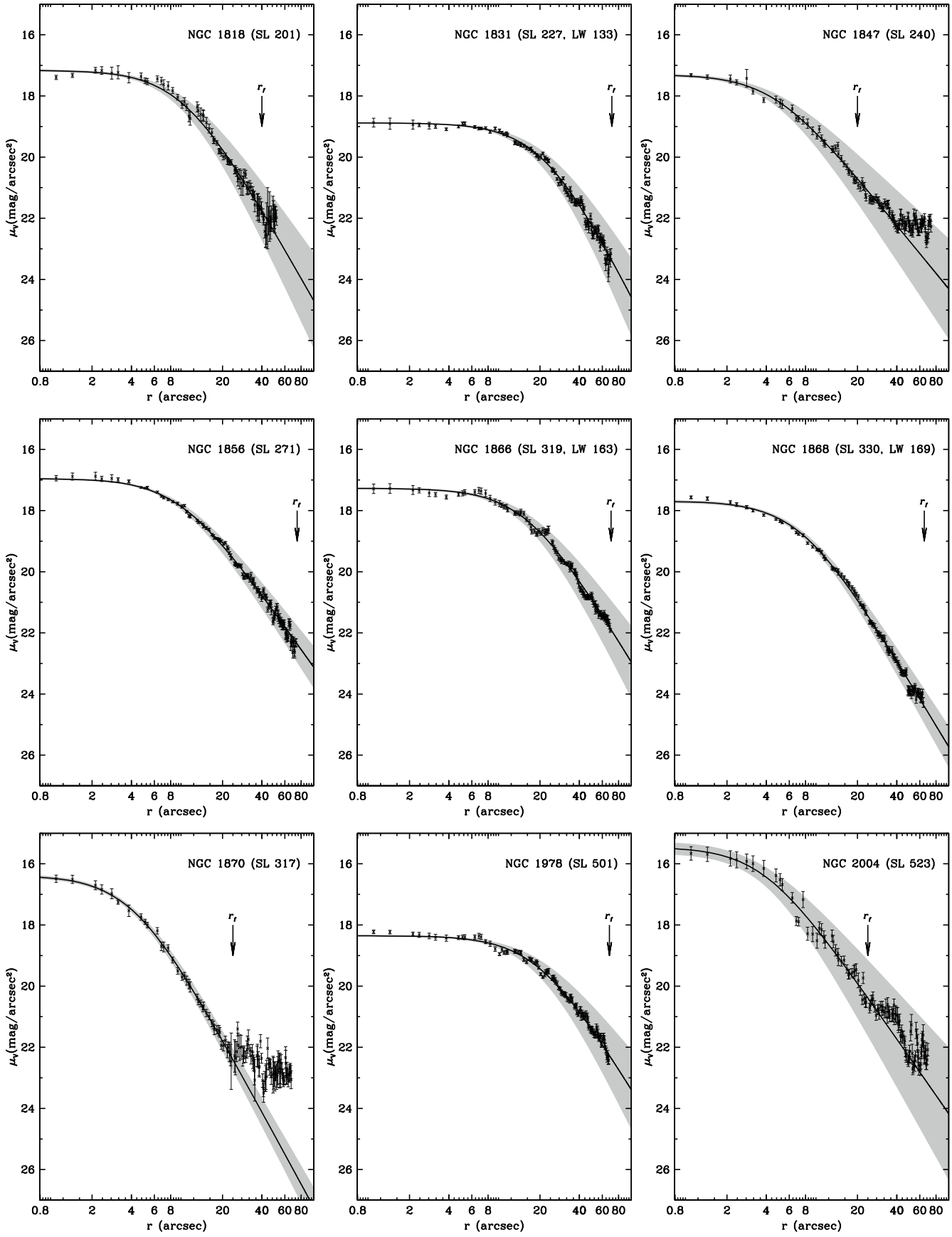

Fig. 3. continued.

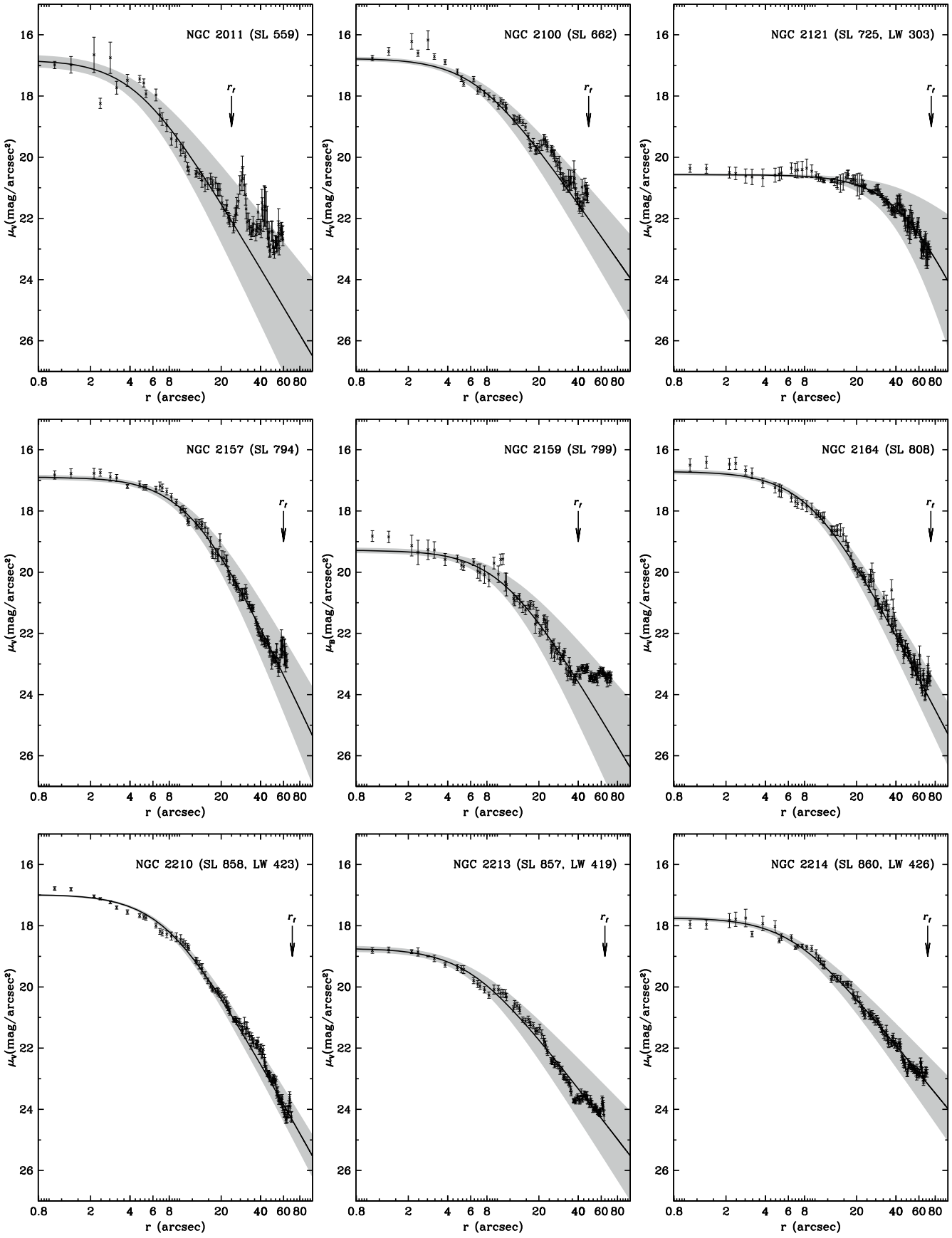

Fig. 3. continued.

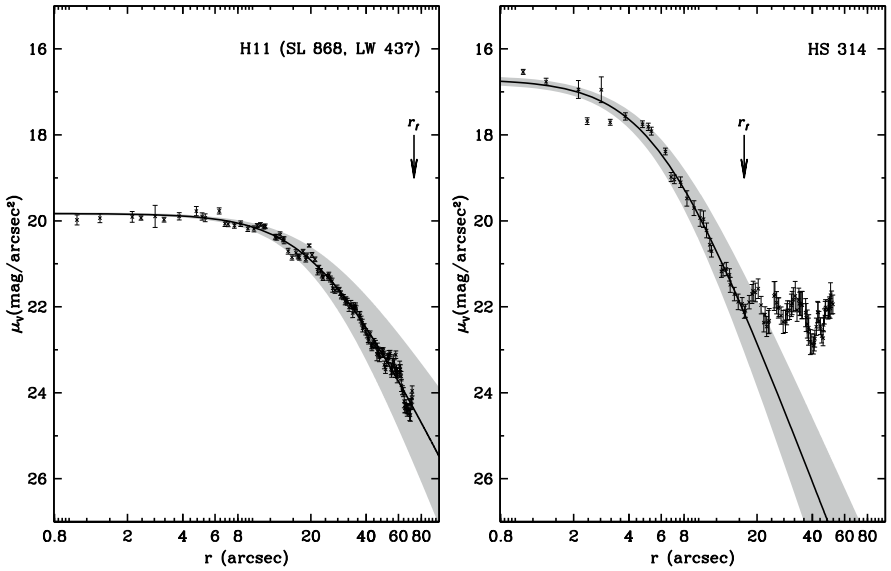

Fig. 3. continued.